KAPL-P-000185
(K97086)

INFRARED MATERIALS FOR THERMOPHOTOVOLTAIC APPLICATIONS

G. W. Charache, J. L. Egley, et. al.

June 1997

NOTICE

KAPL ATOMIC POWER LABORATORY SCHENECTADY, NEW YORK 10701

Operated for the U. S. Department of Energy
by KAPL, Inc. a Lockheed Martin company

Infrared Materials for Thermophotovoltaic Applications

G.W. Charache, J.L. Egley, D.M. Depoy, L.R. Danielson, M.J. Freeman,
R.J. Dziendziel, J.F. Moynihan, P.F. Baldasaro, and B.C. Campbell
Lockheed-Martin, Inc., Schenectady, NY 12301-1072

C.A. Wang, H.K. Choi and G.W. Turner
Lincoln Laboratory, Massachusetts Institute of Technology, Lexington, MA 02173-9108

S.J. Wojtczuk, P. Colter
Spire Corp., Bedford, MA 01730

P. Sharps and M. Timmons
Research Triangle Institute, Research Triangle Park, NC 27709-2194

R.E. Fahey and K. Zhang
OFC Corp., Natick, MA 01760

Abstract

Thermophotovoltaic generation of electricity is attracting renewed attention due to recent advances in low bandgap (0.5-0.7 eV) III-V semiconductors. The use of these devices in a number of applications has been reviewed in a number of sources [1-3]. Two potential low-bandgap diode materials are $In_xGa_{1-x}As_ySb_{1-y}$ and $In_xGa_{1-x}As$. The performance of these devices are comparable (quantum efficiency, open circuit voltage, fill factor) despite the latter's long-term development for optoelectronics. For an 1100 °*C* blackbody, nominally 0.55 eV devices at 25 °*C* exhibit average photon-weighted internal quantum efficiencies of 70-80%, open circuit voltage factors of 60-65%, and fill factors of 65-70%.

Equally as important as the energy conversion device is the spectral control device that effectively transmits the above bandgap radiation into the diode and reflects the below bandgap radiation back to the radiator. Recent developments in spectral control technology, including, InGaAs plasma filters and non-absorbing interference filters are presented. Current tandem filters exhibit spectral utilization factors of ~65% for an 1100 °*C* blackbody.

Introduction

Thermophotovoltaic (TPV) generation of electricity offers fundamental advantages relative to other direct energy conversion techniques (e.g., thermoelectric, thermionic). The most important is the ability to recuperate the low energy waste heat. This allows theoretical conversion efficiencies to approach that of conventional heat engines (e.g., Brayton, Stirling, Rankine). However, experimental achievement of radiator-to-electric conversion efficiencies greater than 20% has not yet been achieved for a blackbody radiator spectrum and a cell-filter combination. Recent advances in low bandgap (0.5-0.7 eV) III-V semiconductors and infrared optics have renewed interest in the development of highly efficient and power dense thermophotovoltaic generation of electricity [1-4].

The efficiency of a thermophotovoltaic energy conversion system is given by [5-7]:

$$\eta = \overline{QE} \cdot \frac{V_{oc}}{E_g} \cdot FF \cdot F_o \cdot F_u \cdot$$

The average photon-weighted quantum efficiency, $\overline{QE}$, is given by,

$$\overline{QE} = \frac{\int_0^{\lambda_g} QE_{internal}(\lambda) N_1(\lambda) d\lambda}{\int_0^{\lambda_g} N_1(\lambda) d\lambda},$$

where, $QE_{internal}(\lambda)$, is the measured internal quantum efficiency spectrum and $N_1(\lambda)$ is the photon flux spectrum absorbed in the TPV cell, which for a blackbody radiator is given by,

$$N_1(\lambda) = \frac{2\pi c \cdot \varepsilon_{rad}(\lambda)}{\lambda^4 \cdot \left(\exp\left(\frac{hc}{kT_{rad}\lambda}\right) - 1\right)} \cdot (1 - R(\lambda) - \alpha(\lambda)),$$

where h is Planck's constant, c is the speed of light, k is Boltzmann's constant, T_{rad} is the blackbody radiator temperature, $\varepsilon_{rad}(\lambda)$ is the emissivity spectrum of the blackbody, $R(\lambda)$ is the net reflection spectra for the TPV cell-filter combination and $\alpha(\lambda)$ the measured absorption spectra of above bandgap photons within a front-surface filter. V_{oc} is the measured open circuit voltage, E_g is the semiconductor bandgap; while the ratio of these quantities is referred to as the open circuit voltage factor. FF is the measured fill factor. Both the voltage factor and fill factor are strong functions of short circuit current and cell temperature The overexcitation factor, F_o, which is the usable fraction of thermal radiation with energy greater than the bandgap, is given by,

$$F_o = \frac{E_g \int_0^{\lambda_g} N_1(\lambda) d\lambda}{\int_0^{\lambda_g} N_2(\lambda) d\lambda},$$

where the energy flux spectrum absorbed in the TPV cell , $N_2(\lambda)$, is the photon flux spectrum multiplied by the energy per photon (i.e., $N_2(\lambda) = N_1(\lambda) \cdot hc/\lambda$). The overexcitation factor is ~ 0.8 for an 1100 $^\circ C$ blackbody and a bandgap of 0.55 eV. The spectral utilization factor, F_u, which is the fraction of total absorbed radiation with energy greater than the bandgap is given by,

$$F_u = \frac{\int_0^{\lambda_g} N_2(\lambda)d\lambda}{\int_0^{\infty} \frac{1-R(\lambda)}{1-R(\lambda)-\alpha(\lambda)} N_2(\lambda)d\lambda}.$$

Simultaneous optimization of all these components is required for a highly efficient TPV system. Table 1 shows previously achieved values for 0.55 eV InGaAs TPV cells with an Si-SiO interference filter for a radiator temperature of 1100 $°C$ and a cell temperature of 25 $°C$ [6]. In comparison to photovoltaic cells (E_g ~ 1.0 - 1.4 eV) matched to the solar spectrum (T_{rad} ~ 5700 $°C$), TPV cells have lower bandgaps (E_g ~ 0.5 - 0.7 eV) and corresponding lower voltage factors and fill factors due to higher dark currents. These losses in efficiency are compensated by increases in both the overexcitation factor and spectral utilization factor, due to the ability to recuperate below bandgap photons with appropriate spectral control filters. Recent advances in both the energy conversion devices and spectral control devices demonstrate that > 20% efficient devices may be achievable.

Energy Conversion Devices

A number of low bandgap materials have been investigated for thermophotovoltaic energy conversion including: Ge, GaSb, InGaAs, InGaSb, and InGaAsSb. Of these, InGaAs grown lattice-mismatched on InP substrates and InGaAsSb grown lattice-matched on GaSb substrates have demonstrated the highest performance for nominally 0.55 eV bandgaps. Figure 1 illustrates typical device architectures for these material systems. In both cases, the p-type layer

is utilized as the absorption layer due to the higher minority carrier diffusion lengths relative to n-type material. However, since shallow n-type ohmic contacts have not yet been developed for Sb-based devices, a thick p-type emitter is utilized for the InGaAsSb cell. For both devices, performance is dominated by surface/interface recombination velocities. In the case of n-on-p InGaAs devices, the back surface field is the critical layer, while for p-on-n InGaAsSb devices, the window is the critical layer. All results shown in Figs. 2-4 are for 1 cm^2 devices.

Figure 2 compares the external quantum efficiency of nominally 0.55 eV InGaAs and InGaAsSb TPV cells. InGaAs devices were grown by organometallic vapor phase epitaxy (OMVPE), while the InGaAsSb devices were grown by both molecular beam epitaxy (MBE) and OMVPE. Details of the growth processes have been described elsewhere [8-9]. None of the devices shown in Fig. 2 have anti-reflection coatings. The surface reflection is ~32-33%, and 36-39% over the 1-2.2 μm range for the InGaAs and InGaAsSb, respectively. This yields $\overline{QE}$ values of 0.68 and 0.79 for the InGaAs and InGaAsSb devices, respectively. Due to the large number of photons near the band-edge, the value of internal quantum efficiency between 1.9 and 2.2 μm, dominates the $\overline{QE}$ value. Modeled QE(λ) results have yielded diffusion lengths of ~ 9 μm for p-InGaAs (0.55 eV) and > 10 μm for p-InGaAsSb (0.55 eV).

The open circuit voltage factors versus short circuit current density at 25 °C for the same devices are shown in Figure 3 in comparison to the radiative limit [10]. This data was obtained by varying the intensity of a light source on devices soldered to a copper heat sink. Device temperature was monitored by a thermocouple mounted in the copper heat sink and temperature was controlled with a thermoelectric cooler. As evidenced in Figure 3, the open circuit voltage

factor increases as the short circuit current increases. Typical current density levels for an 1100 $^{\circ}C$ blackbody source are 3 - 5 A/cm^2. Thus, voltage factors for both InGaAsSb and InGaAs are 60-65% for devices operating at 25 $^{\circ}C$.

Figure 4 plots the measured fill factor versus short circuit current density for both InGaAs and InGaAsSb devices. Maximum achievable fill factors assuming radiative limited dark current for 0.55 eV devices is ~70%. As seen in Fig. 4, fill factors are not currently limited by series resistance for either material system up to approximately 1 A/cm^2. Beyond this current level further improvements in front grid design and processing are required for both devices.

The reliability of lattice-mismatched InGaAs TPV devices was investigated by operating these devices continuously in the LED-mode (forward-bias) under constant dc-current and temperature conditions in air. Devices were mounted and monitored in a similar method to the V_{oc}/E_g versus I_{sc} measurements. Periodically, the devices were characterized by measuring the non-illuminated current versus voltage curve, in order to check degradation in the dark current or series resistance. Currently, devices operating at 30 $^{\circ}C$ and 3 A/cm^2, 100 $^{\circ}C$ and 7 A/cm^2, and 100 $^{\circ}C$ and 20 A/cm^2 have logged over 4000, 3000, and 500 hours, respectively, without degradation.

Spectral Control Devices

The two main categories of spectral control devices for a blackbody radiator are frontside (between the source and cell) and backside (underneath the cell). Both types of devices reflect the below bandgap radiation back to the source with minimal absorption. A summary of the advantages/

disadvantages of each of these techniques are shown in Table 2. In addition to these, a backside reflector has a number of potential advantages that improve the intrinsic TPV device performance, such as: improved collection efficiency, increased optical absorption, and photon recycling. These advantages lead to the following TPV cell improvements: enhanced short circuit current, increased open circuit voltage and reduced sensitivity to material quality [11]. The use of back surface spectral control devices for thermophotovoltaic applications has been reviewed elsewhere [12]. Current back surface reflector device designs are limited by trade-offs between free carrier absorption and high reflectivity.

Front surface spectral control devices include both interference filters and plasma filters. Interference filters consist of alternating layers of dielectric materials that vary in index of refraction. Their thicknesses and refractive indices are chosen to obtain a high degree of reflection (> 95%) over a selected wavelength range and a high transmission elsewhere. Unfortunately, as the wavelength range increases, the complexity and number of dielectric layers also increases [13]. Thus, since a TPV spectral control device requires a high reflection from ~2 μm to 10 μm, an interference filter cannot perform alone. The use of an interference/plasma tandem filter becomes a desirable alternative. In addition, when coupled to a plasma filter, the materials utilized must be non-absorbing over the entire 1.1-10 μm wavelength range.

Front surface plasma filters have been implemented with transparent conducting oxides, and heavily-doped semiconductors [1,2]. The most successful of these has been the use of heavily-doped InGaAs [14]. Due to the high carrier concentrations that have been obtained in $In_xGa_{1-x}As$ and low electron effective mass, both the Moss-Burstein optical bandgap shift and plasma reflection characteristics are expected to be particularly dramatic. Higher electrically active

carrier concentrations are observed as the indium fraction increases. Thus, carrier concentrations approaching 10^{20} cm^{-3} should be readily attained with a variety of dopant sources for indium fractions greater than 0.53 percent [14].

Figure 5 illustrates the effective photonic bandgap as a function of doping level for $In_{0.67}Ga_{0.33}As$. The measured photonic bandgap along with calculated values for both parabolic and non-parabolic band approximations are included [14]. The deviation of the measured and calculated values at doping levels greater than 10^{19} cm^{-3} may be due to two effects: filling of the satellite L-valley and bandgap narrowing. The position of the L-valley in $In_{0.67}Ga_{0.33}As$ was estimated from published values of the L-valley bandgap in GaAs (E_g = 1.70 - 1.73 eV) and InAs (E_g = 1.07 - 1.43 eV) [16-18] and the L-valley bowing parameter (c ~ 0.5 eV) [15,17]. Depending on the position of the L-valley in InAs, the L-valley bandgap in $In_{0.67}Ga_{0.33}As$ can range from 1.16 - 1.6 eV. The lower end of this range may effect the measured photonic bandgap as shown in Fig. 5. Thus, it is unclear whether filling of the satellite valley or bandgap narrowing is the dominant effect.

Figure 6 plots the measured plasma reflection characteristics for $In_{0.67}Ga_{0.33}As$. These films demonstrate the characteristic plasma-edge shift toward shorter wavelengths as the free-electron concentration increases. The sharp turn-on of the sample doped 5×10^{19} cm^{-3} is due to the high mobility (low effective mass) of $In_{0.67}Ga_{0.33}As$. Modeling the reflection characteristics of these films with the Drude-theory allows the extraction of the below-bandgap optical constants [14]. Both modeled and measured data have shown that these InGaAs plasma filters demonstrate high

below-bandgap reflection and negligible above-bandgap absorption due to the combined effects of the Moss-Burstein shift and plasma reflection.

These films coupled with an appropriate non-absorbing interference filter yield a highly effective tandem filter concept for TPV spectral control. Figure 7 illustrates the reflection versus wavelength for an initial tandem filter concept. For this concept, an interference filter was directly deposited on the InGaAs plasma and an anti-reflection (AR) coating was deposited on the backside of the InP substrate, to maximize above-bandgap transmission. This filter demonstrates a spectral utilization factor of ~65% for a 1100 $^{\circ}C$ blackbody radiator.

Conclusions

Current 0.55 eV lattice-mismatched InGaAs:InP and lattice-matched InGaAsSb:GaSb demonstrate similar thermophotovoltaic efficiencies (η = 14 - 16%) at 1100 $^{\circ}C$ radiator temperatures. In addition, both material systems have been grown utilizing a number of growth techniques and are expected to demonstrate high-reliability at typical operating conditions (> 10^5 hours, 1-10 A/cm^2, 50-100 $^{\circ}C$). Primary advantages of InGaAs devices are its long-term infrastructure development for optoelectronic applications and its demonstrated mass-reproducibility. Antimonide-based TPV devices may offer longer-term device advantages due to simpler device structure and demonstrated longer diffusion lengths.

High performance (η > 20%) TPV devices may utilize both a front surface filter for below-bandgap spectral control and a back-surface reflector for TPV device-related improvements. Currently, front-surface tandem filters have demonstrated spectral utilization factors of ~ 65%

for an 1100 $^{\circ}C$ blackbody radiator. Further improvements in either the plasma filter or non-absorbing interference filter are required in order to reduce absorption in the 4-7 μm wavelength region.

References

[1] T. J. Coutts, J. P. Benner, Eds., *The First NREL Conference on Thermophotovoltaic Generation of Electricity*, AIP Conference Proceedings **321**, American Institute of Physics, New York, 1994.

[2] J. P. Benner, T. J. Coutts, D. S. Ginley, Eds., *The Second NREL Conference on Thermophotovoltaic Generation of Electricity*, AIP Conference Proceedings **358**, American Institute of Physics, New York, 1995.

[3] T. J. Coutts, M. W. Wanlass, J. S. Ward, and S. Johnson, "A Review of Recent Advances in Thermophotovoltaics," *25th IEEE Photovoltaics Specialist Conference*, 25 (1996).

[4] The Third NREL Conference on the Thermophotovoltaic Generation of Electricity, Colorado Springs, CO (1997).

[5] L.D. Woolf, "Optimum Efficiency of Single and Multiple Junction Bandgap Cells for Thermophotovoltaic Energy Conversion," Solar Cells, **19**, 19 (1986).

[6] G.W. Charache, D.M. DePoy, M. Zierak, J.M. Borrego, P.F. Baldasaro, J.R. Parrington, M.J. Freeman, E.J. Brown, M.A. Postlethwait, and G.J. Nichols, "Measurement of Conversion Efficiency of Thermophotovoltaic Devices,", *The Second NREL Conference on Thermophotovoltaic Generation of Electricity*, AIP Conference Proceedings **358**, 351 (1995).

[7] P.F. Baldasaro, E.J. Brown, D.M. DePoy, B.C. Campbell and J.R. Parrington, "Experimental Assessment of Low Temperature Voltaic Energy Conversion," *The First NREL Conference on*

Thermophotovoltaic Generation of Electricity, AIP Conference Proceedings **321**, 29 (1994).

[8] S.J. Wojtczuk, P. Colter, G. Charache, and B. Campbell, "Production Data on 0.55 eV InGaAs Thermophotovoltaic Cells," *25th IEEE Photovoltaics Specialist Conference*, 77 (1996).

[9] C.A. Wang, H.K. Choi, G.W. Turner, D.L. Spears, M.J. Manfra, and G.W. Charache, "Lattice-Matched Epitaxial GaInAsSb/GaSb Thermophotovoltaic Devices," The Third NREL Conference on the Thermophotovoltaic Generation of Electricity, Colorado Springs, CO (1997).

[10] C.H. Henry, "Limiting Efficiencies of Ideal Single and Multiple Energy Gap Terrestrial Solar Cells," Jl. Appl. Phys., **51**, 4494 (1980).

[11] C.B. Honsberg and A.M. Barnett, "Light Trapping in Thin Film GaAs Solar Cells," *22nd IEEE Photovoltaics Specialist Conference*, 262 (1991).

[12] G.W. Charache, D.M. DePoy, P.F. Baldasaro, and B.C.' Campbell, "Thermophotovoltaic Devices Utilizing a Back Surface Reflector for Spectral Control," *The Second NREL Conference on Thermophotovoltaic Generation of Electricity*, AIP Conference Proceedings **358**, 339 (1995).

[13] A. Thelen, "Multilayer Filters with Wide Transmittance Bands," Jl. Opt. Soc. Amer., **53**, 1266 (1963).

[14] G.W. Charache, D.M. DePoy, J.L. Egley, R.J. Dziendziel, M.J. Freeman, P.F. Baldasaro, and B.C. Campbell, P.R. Sharps, M.L. Timmons, R.E. Fahey, K. Zhang, and J.M. Borrego, "Electrical and Optical Properties of Degenerately-Doped N-Type InGaAs," The Third NREL

Conference on the Thermophotovoltaic Generation of Electricity, Colorado Springs, CO (1997).

[15] V.M. Glazov, R.A. Akopyan, and E.I. Sgvedkov, "Investigation of the Relationship Between the Electron Density and Solubilities of Sulfur, Selenium and Tellurium in Indium Arsenide," Sov. Phys. Semicond., **10**, 378 (1976).

[16] S. Tiwari and D.J. Frank, "Empirical Fit to Band Discontinuities and Barrier Heights in III-V Alloy System", *Appl. Phys. Lett.*, **60**, 630 (1992).

[17] M. Levenshtei, R. Rumyantsev, and M. Shur, Eds., *Handbook Series on Semiconductor Parameters vol. 1*, New York: World Scientific, 1996.

[18] S. Adachi, "Bandgaps and Refractive Indices of AlGaAsSb, GaInAsSb, and InPAsSb: Key Properties for a Variety of the 2-4 μm Optoelectronic Device Applications", *Jl. Appl. Phys.*, **61**, 4869 (1987).

Table 1 - TPV Cell / Filter Efficiency Components

Cell / Filter	$\overline{QE}$	V_{oc}/E_g	FF	F_o	F_u	η
InGaAs / Interference	0.68	0.63	0.68	0.8	0.6	14%*
InGaAsSb / Tandem	0.78	0.63	0.65	0.8	0.65	16%**
Limit	1.0	0.7	0.7	0.8	1.0	40%

* Independently measured with integral heat absorption measurements [6]
** Only differential measurements performed

Table 2 - Advantages and Disadvantages of Spectral Control Options

Spectral Control Option	Advantage	Disadvantage
Frontside	Free carrier absorption in voltaic diode not an issue. Independent design of voltaic diode and spectral control device.	Must be highly transmissive to above bandgap photons.
Backside	Absorption of above bandgap photons is not an issue. Higher voltaic diode power density.	Free carrier absorption in diode requires device design alterations - this leads to increased series resistance

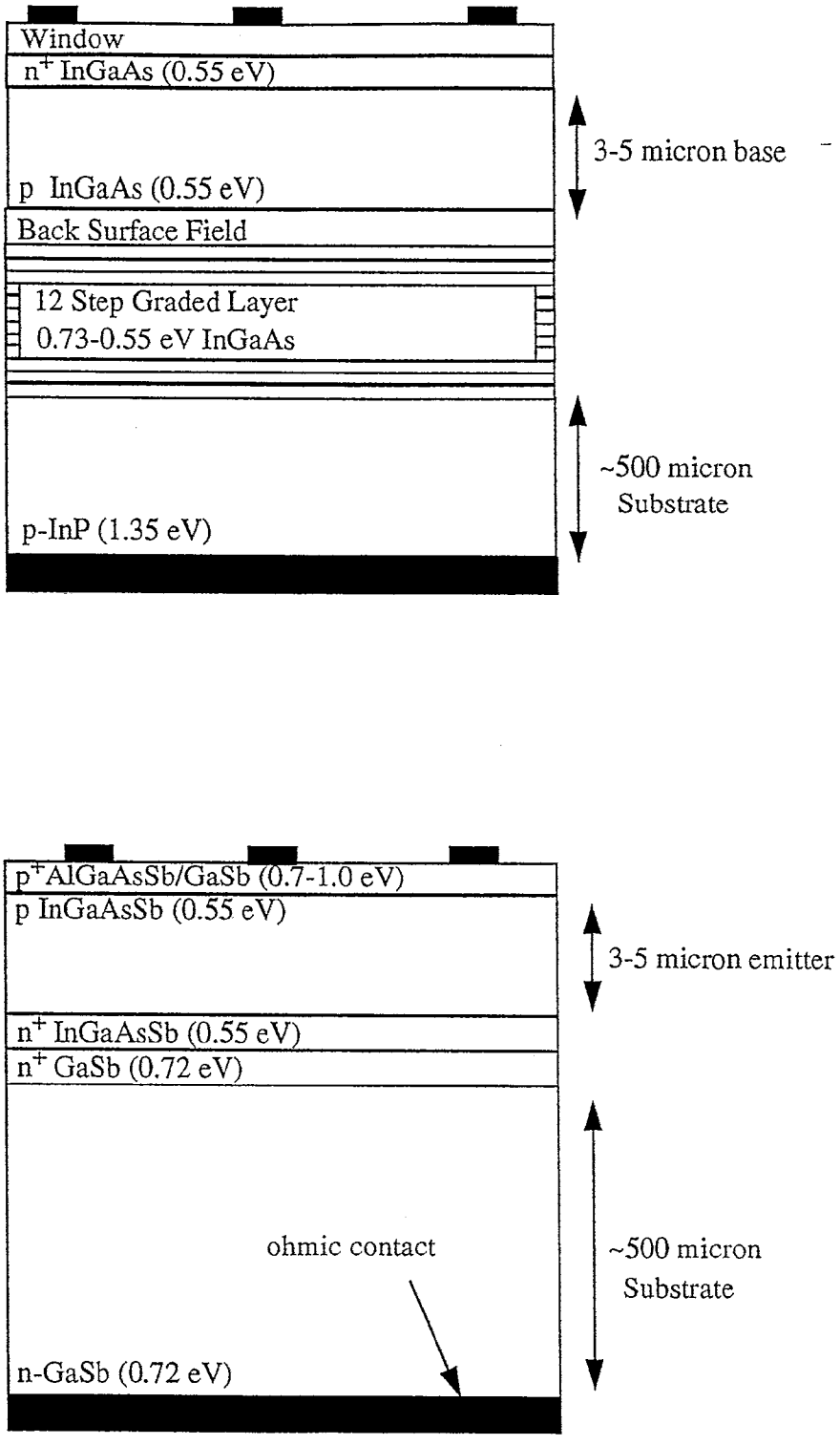

Figure 1 - 0.55 eV InGaAs and InGaAsSb TPV device architectures.

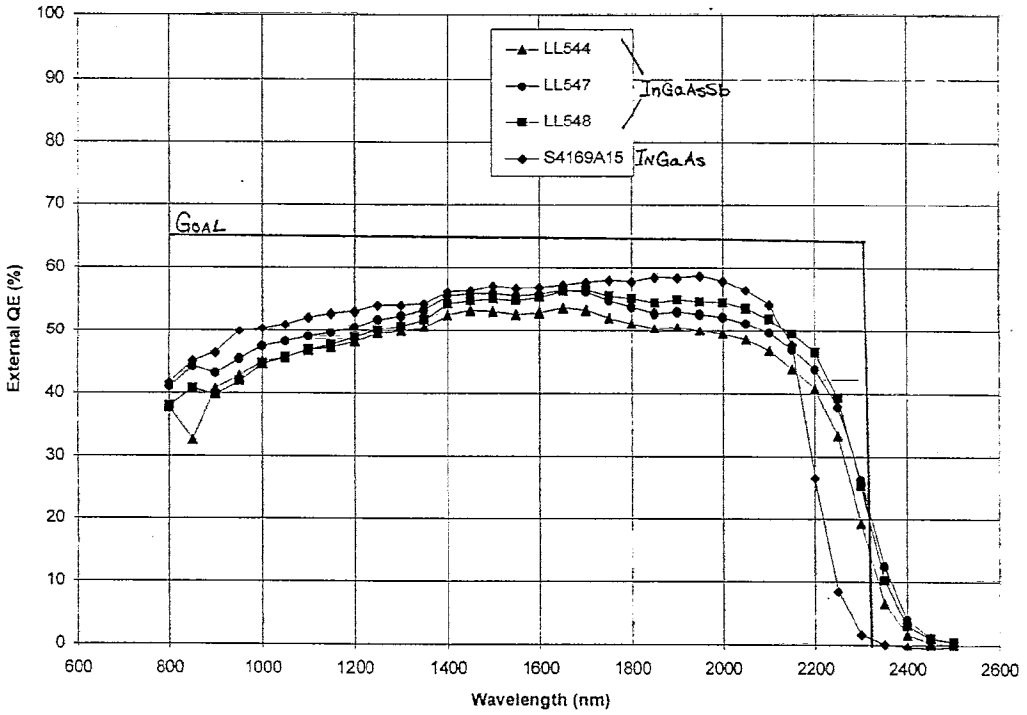

Figure 2 - Comparison of external quantum efficiency of nominally 0.55 eV InGaAs and InGaAsSb TPV diodes (no anti-reflection coating).

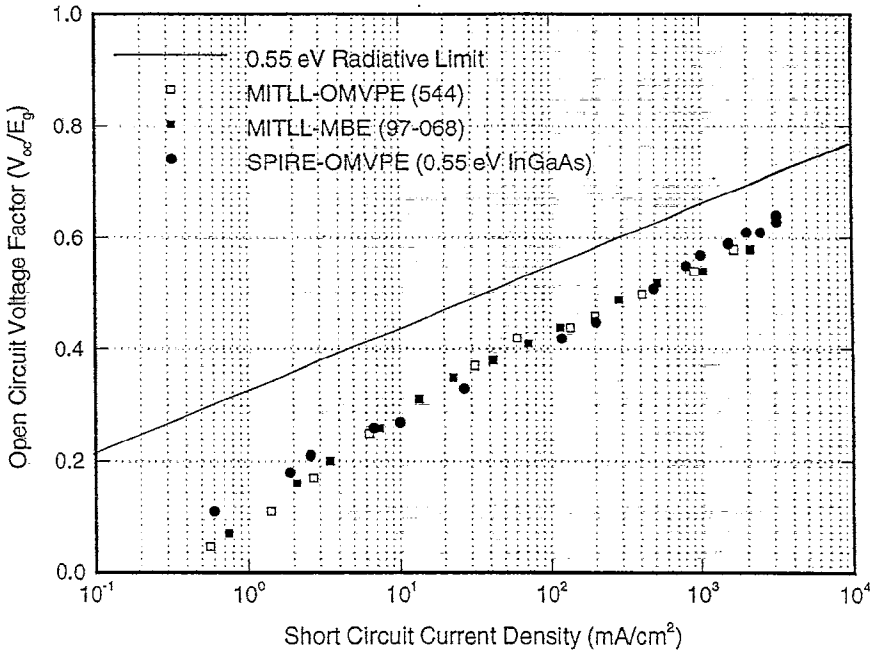

Figure 3- Comparison of the open circuit voltage factor versus short circuit current of nominally 0.55 eV InGaAs and InGaAsSb TPV diodes.

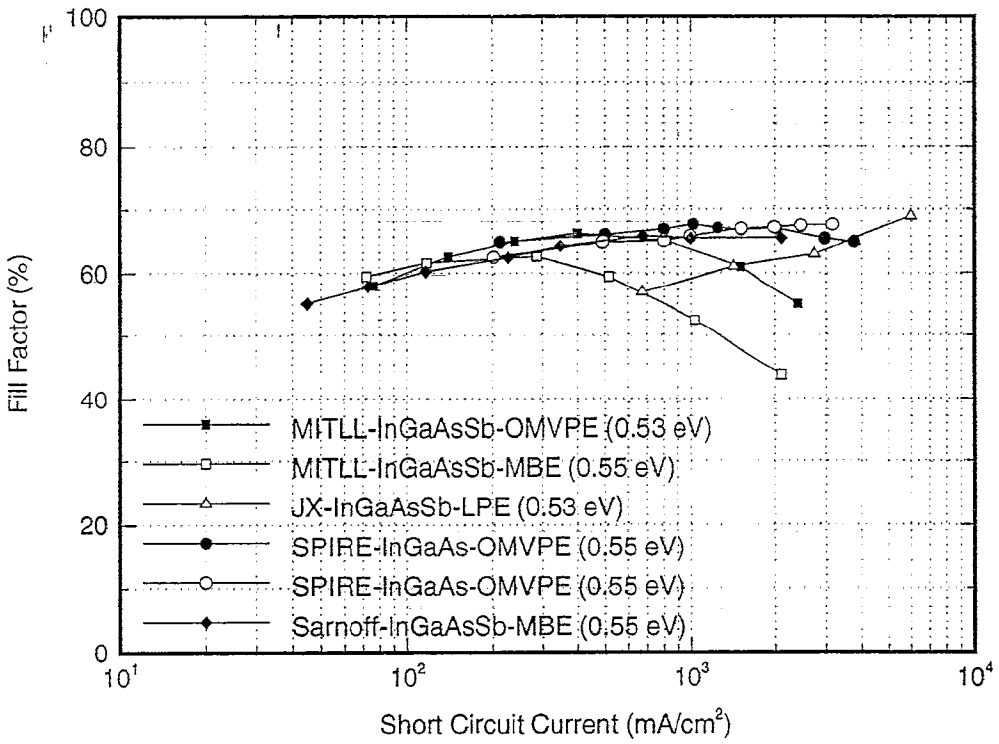

Figure 4 - Comparison of the fill factor versus short circuit current of nominally 0.55 eV InGaAs and InGaAsSb TPV diodes.

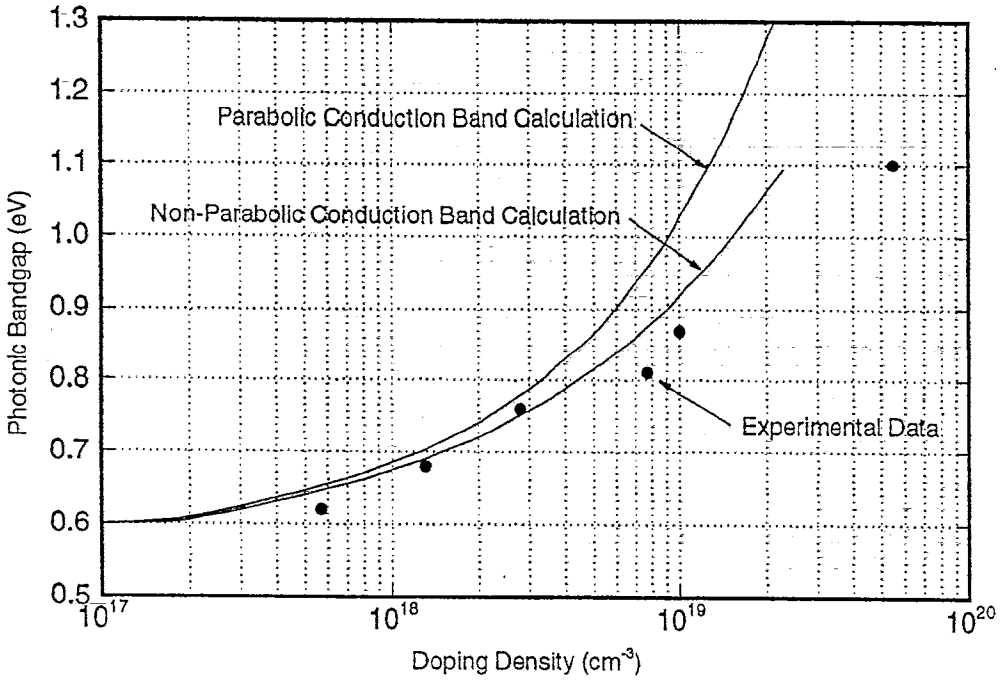

Figure 5 - Theoretical and measured values of the effective photonic bandgap for 0.6 eV InGaAs.

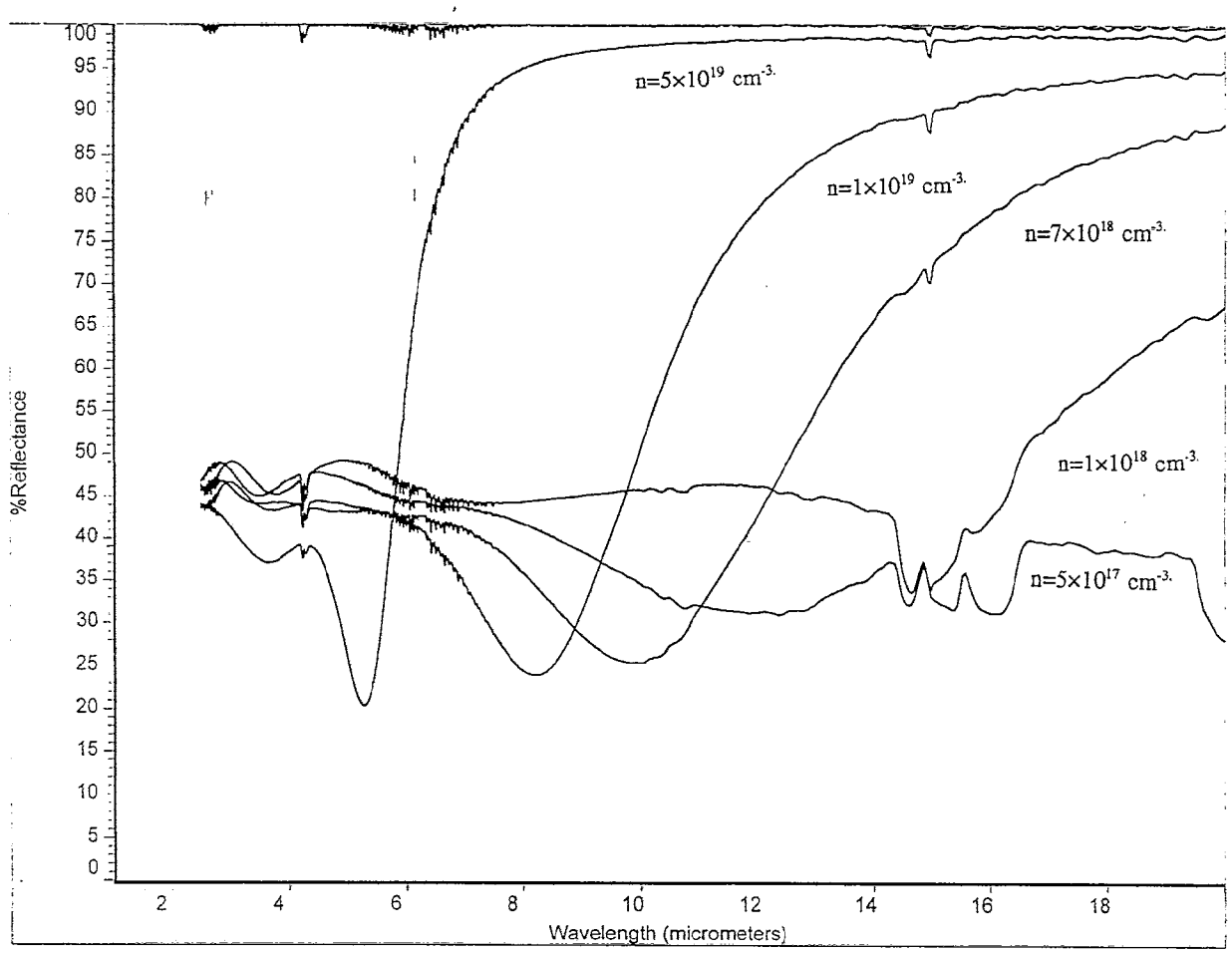

Figure 6 - Measured plasma reflection characteristic of 0.6 eV InGaAs.

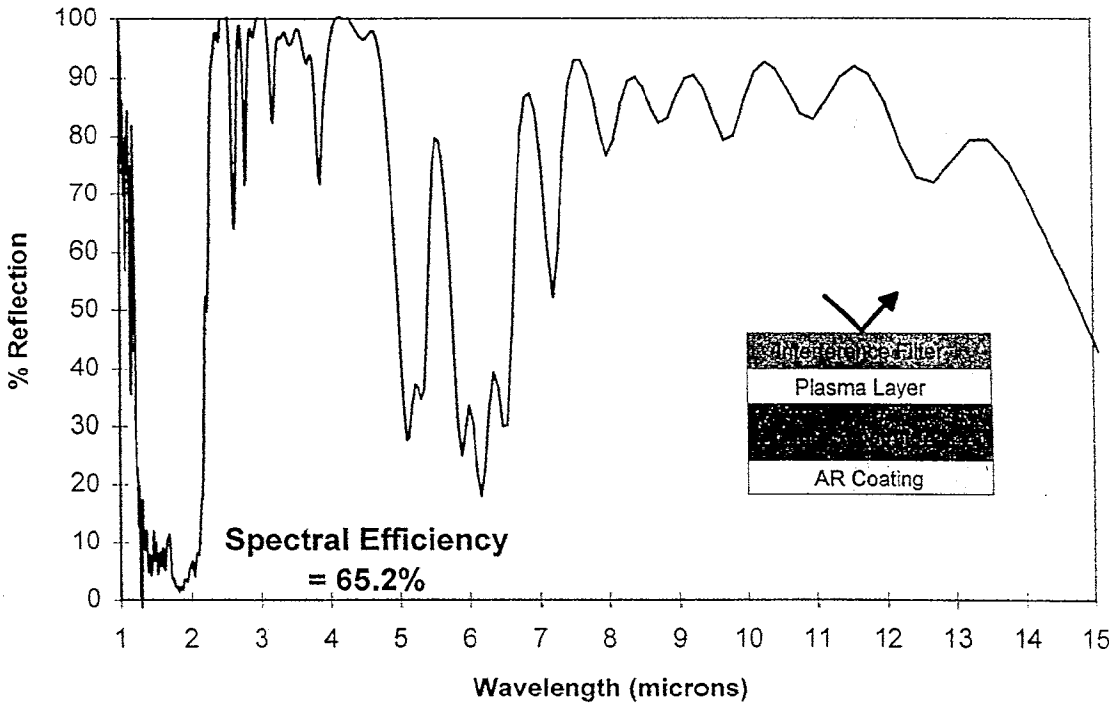

Figure 7 - Measured reflection versus wavelength for a 0.6 eV InGaAs plasma / non-absorbing interference filter tandem filter.